4-29-2019

Inferring Glaciological Attributes of Thwaites Glacier Using GPS-Interferometric Reflectometry and Precise Point Positioning

Peter Ogden Matheny

INFERRING GLACIOLOGICAL ATTRIBUTES OF THWAITES GLACIER USING GPS-INTERFEROMETRIC REFLECTOMETRY AND PRECISE POINT POSITIONING

by

Peter Matheny

A Thesis

Submitted in Partial Fulfillment of the

Requirements for the Degree of

Master of Science

Major: Earth Sciences

The University of Memphis
May 2019

Acknowledgments

I greatly appreciate Dr. Smalley, my mentor and adviser, for supporting me throughout this process. He introduced me to geodetic sciences, a field I had been unwittingly searching for during my academic career. Working with Dr. Smalley has allowed me practical experiences that helped expand my learning beyond the classroom. I have been fortunate in my work with Dr. Smalley to travel to places I never imagined I would visit and meet with people who have enhanced my professional developmental. It has been these unique experiences that made this project possible. I look forward to collaborating with Dr. Smalley in the future as I continue in my career in geophysics. Further, the feedback and guidance provided by my committee, Eric Daub and Chuck Langston, have helped to enhance the quality of this project. I am honored to have worked with so many people at the Center for Earthquake Research and Information (CERI) who have greatly contributed to my professional growth and development.

I would like to express my gratitude to Terry Wilson and the rest of the team on the POLENET project for providing the foundation for my thesis through data collection at GPS stations in Antarctica. My gratitude extends beyond having access to analyze the GPS data to the tremendous opportunity Dr. Wilson provided for me to service the GPS stations in Antarctica. It was this hands-on experience that enhanced my awareness of the meaning and impact my project could have on the broader scientific community. It was this tangible fieldwork that cultivated a budding passion of mine to contribute to geophysics research in Antarctica.

There were many people and facilities that made the data processing and analysis for this project possible. For instance, I would like to thank Brooke Medley for making a snow accumulation grid over Thwaites glacier, creating the infrastructure on which I was able to expand and develop my own project. Additionally, I appreciate Kristine Larson for providing the software I used to process the data. I would also like to thank the UNAVCO and ECMWF for allowing me to access the data I used for this thesis and for making the process of downloading and analyzing that data an easy one.

Finally, I cannot adequately express the gratitude I have for my family and friends

for supporting me throughout the creation and development of this project. It is because of this support that I have been able to persevere after many years of working towards my thesis completion.

Abstract

We use two continuous GPS stations located on Thwaites glacier to estimate the rate of snow accumulation through GPS interferometric reflectometry and separately examine details of the motions of the glacier. We find an 8-year snow accumulation rate in meters water equivalent for the station Upper Thwaites of 0.44±0.03 m.w.e./yr and a 7-year rate for the station Lower Thwaites of 0.56±0.06 m.w.e./yr. Averages at both GPS sites match the European Centre for Medium-Range Weather Forecasts reanalysis accumulation rate, derived from integrated snowfall over the same period. We used precise point positioning to obtain daily station positions and modeled the observed movement of the glacier towards the Amundsen Sea using a constant acceleration and periodic fluctuations about this background motion. Lower Thwaites exhibits statistically significant deviations from this model that may be related to emptying and refilling of a nearby sub-glacial lake.

Table of Contents

List of Figures

Introduction

Background

Thwaites glacier, part of the West Antarctic Ice Sheet (WAIS), is undergoing the most significant changes of any ice-ocean system in Antarctica, leading to a contribution of about 0.1 mm a-1 towards sea level rise. With a broad ice front, below sea level grounding line, and increased thickening inland, Thwaites glacier is likely to retreat, triggering a collapse of WAIS (Scambos et al.). The removal of ice shelves drives instability of Thwaites glacier through increased glacial calving at the ice shelf-ocean boundary, a process that also causes grounding-line retreat (Rignot et al.). The total amount of ice contained in the Thwaites glacier catchment is equivalent to a global sea level rise of 1.2 meters (Medley et al.). Thwaites glacier could collapse in as soon as 200 years. Given its unique capacity to dramatically increase global sea level, studying Thwaites glacier has significant implications on understanding effects of climate change in Antarctica.

The motion of Thwaites glacier is not uniform across the catchment. As a simple approximation, the displacement towards the Amundsen Sea Embayment increases towards the grounding line. Other factors may also play a role in the heterogeneous displacement, such as filling and draining of sub-glacial lakes (Dow et al.). Lakes can form under fast flowing glaciers where basal sliding creates melt-water which fills closed depressions in the surface underneath the glacier(Dow et al.). The latest continent-wide sub-glacial lake inventory by Wright and Siegert found no lakes underneath Thwaites glacier; however a recent study found four interconnected lakes at distances of 70, 124, 142 and 170 kilometers from the Thwaites glacier grounding line (Smith et al.). The authors name the lakes in conjunction with their distance from the grounding line: THW_{70}, THW_{124}, THW_{142}, and THW_{170}. The lakes simultaneously drained from 2013-2014 as determined by Cryo-Sat 2 altimetry data.

The Antarctic component (ANET) of the Polar Earth Observing Network (POLENET) consists of 56 geodetic GPS installations in remote locations across Antarctica, including two on Thwaites glacier that are the focus this study. POLENET, which focuses on the relationship

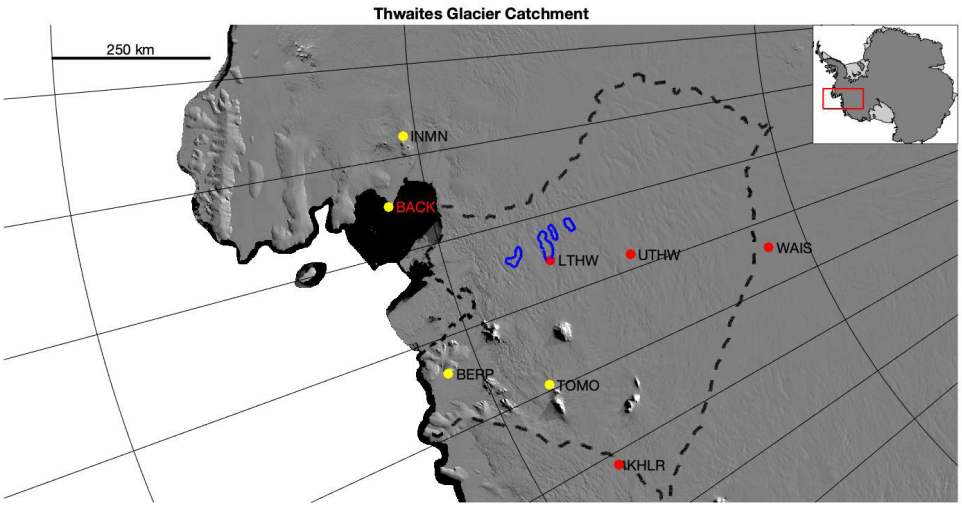

Figure 1 - Map of the Thwaites glacier catchment (black dashed line) from Zwally et al. and all POLENET GPS stations in the region plotted on the Moderate-Resolution Imaging Spectroradiometer (MODIS) digital elevation model (DEM) at very low contrast (Greene et al.). Stations with a red marker are installed on glaciers while yellow markers indicate rock installations. Sub-glacial lakes located in the Thwaites catchment are also shown in blue.

between polar ice sheets and changing sea level, began during the International Polar Year 2007-2008 and is currently in its third phase, which began in the Fall of 2018. Recently, data from ANET has been used to estimate the amount of glacial isostatic adjustment (GIA) in West Antarctica around Thwaites Glacier (Barletta et al.). GIA is the viscoelastic crustal response to ice load changes that is causing crustal elevation changes at the millimeter to centimeter per year scale in Antarctica. POLENET additionally installed a few GPS stations on glaciers in WAIS for glaciological studies. Continuous GPS stations on moving ice can measure glaciological properties difficult to measure by other means. Utilizing the Upper and Lower Thwaites glacier stations (UTHW and LTHW), we focus on determining snow accumulation and, separately, the analysis of the displacement using the standard linear trajectory model (SLTM), which models the displacement history in terms of secular and periodic components (Bevis and Brown). We compare our snow accumulation estimates to those found by three other techniques: global snowfall models, ice-core analysis and other GPS-IR results. Thwaites glacier and its catchment boundary are displayed in Figure 1 with the locations of POLENET GPS stations and the sub-glacial lakes described in Smith et al..

In the remaining sections of Chapter 1, we describe the GPS network, GPS signal

characteristics, and GPS-IR in detail. Chapter 2 includes information on the displacement of both stations and SLTM parameters as well as the specific snow accumulation model parameters used in this study. Chapter 3 offers a detailed analysis and discussion of the results. Finally, Chapter 4 reviews the results and methods of this thesis.

GPS Network

The two stations examined here, UTHW and LTHW, were installed during the first phase of POLENET. UTHW started collecting data on 22 December 2008, while LTHW began collecting data almost a year later on 12 December 2009. While precipitation is relatively low at both sites compared to the up to 1 meter per year in the coastal region of Thwaites glacier, snow still accumulates. By driving a 2-meter aluminum pole half meter into snow most vibrational effects due to high winds are mitigated. Nearby the antenna is a metal frame made of three 2 meter vertical aluminum poles arranged in a triangle that are bolted to a 1-meter square plywood foundation. The antenna and antenna frame are shown in Figure 2. At the top of the frame and fixed to aluminum joists are three solar panels, a wind turbine, a meteorological (MET) package and two satellite antennas. At the base of the metal frame are three hard-plastic cases, which contain 18 evenly distributed lead-acid batteries, heating pads, two satellite modems, and the GPS receiver. Eighteen batteries are required to sustain the 4.0-watt receiver plus antenna and 2 watt dual Iridium modem loads through the sunless austral winter The wind turbine provides an assist and any excess power it generates is dumped into the heating pads to improve battery performance by raising the temperature in the equipment cases. Figure 2 shows before and after pictures of the antenna at UTHW during a site visit on 9 January 2018 during which the antenna was found covered in a thin layer of snow and subsequently raised.

Site visits were initially planned for every two years; however, maintenance teams were able to reach the sites more often. A typical site visit consists of raising the receiver frame and antenna, possibly updating the receiver firmware, and replacing failing batteries. The new antenna heights, after a raise, were not always recorded; Table 1 lists site visits and available antenna height raise information relative to the snow surface around the antenna.

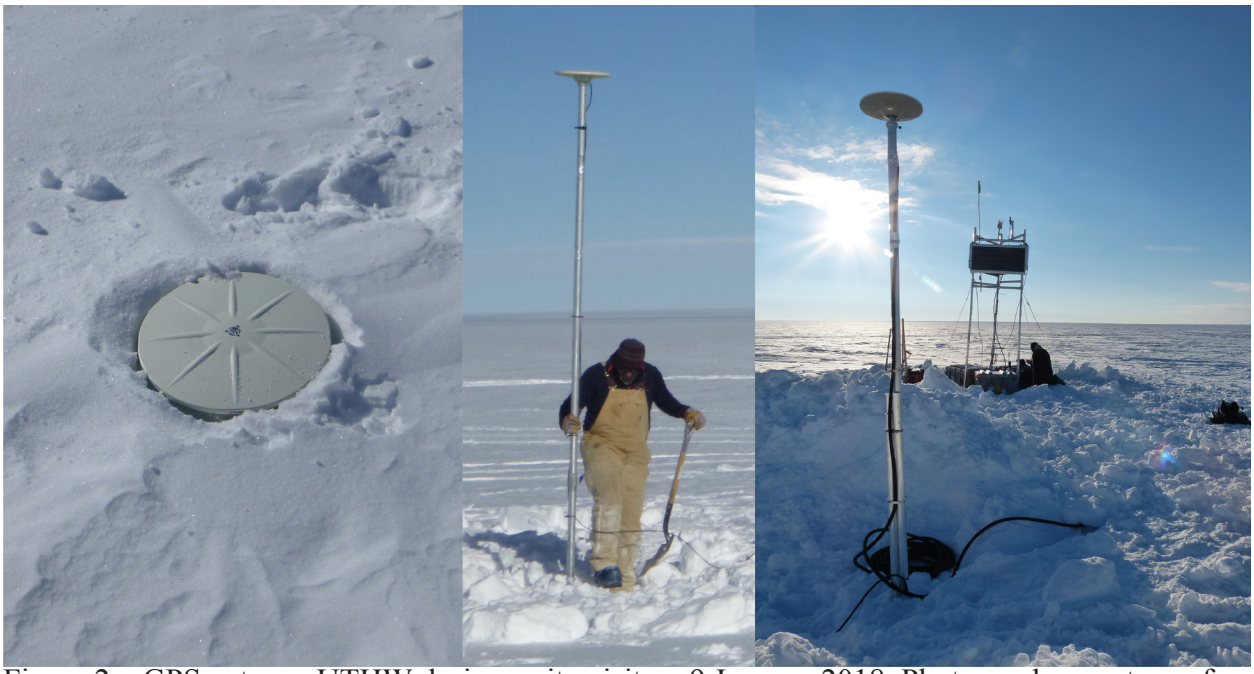

Figure 2 – GPS antenna UTHW during a site visit on 9 January 2018. Photographs courtesy of David Saddler.

The receivers record pseudo-range, phase, and signal strength every thirty seconds. Raw data in proprietary NetRS format from both stations are telemetered daily via Iridium satellite to UNAVCO, Inc. headquarters in Boulder, Colorado and converted into the international standard Receiver Independent Exchange (RINEX) format version 2.11 (Gurtner and Estey). The data is then made available for download via UNAVCO's Data Archive Interface version 2 (DAIv2). Stored alongside observational RINEX files are navigation and MET files at UNAVCO. The navigational files allow us to find the azimuth and elevation of the satellite relative to the antenna once the antenna's position is known. Up until the 2014-2015 season visit, there was an elevation mask of 7 degrees, meaning the receivers did not record direct signals from below 7 degrees elevation. Data collected by the MET pack on both sites are stored in a meteorological RINEX file with the pressure, dry temperature, relative humidity, wind speed, and wind direction.

After retrieving data from the DAIv2, it is processed at the University of Memphis, using the Natural Resources Canada (NRCan) precise point positioning (PPP) software. NRCan PPP uses precise satellite orbits, that are two orders of magnitude more precise than the broadcast orbits, to estimate the position of the GPS station in the International Terrestrial Reference

Table 1 – Site visit dates noting both known and unknown antenna raisings. The first and third visit date listing correspond to UTHW information while the second and fourth are for LTHW.

Visit Date (UTHW)	22-Dec-08	-	14-Jan-11	23-Dec-11	10-Dec-12
Action Taken	Installed	-	Raised	Raised	-
Antenna Height (m)	-	-	-	1.542	-
Visit Date (LTHW)	-	12-Dec-09	-	13-Jan-12	12-Dec-12
Action Taken	-	Installed	-	Raised	Raised
Antenna Height (m)	-	-	-	1.856	0.832
Season	2013-2014	2014-2015	2015-2016	2016-2017	
Visit Date (UTHW)	-	9-Jan-15	12-Jan-16	-	
Action Taken	-	Raised	-	-	
Antenna Height (m)	-	-	-	-	
Visit Date (LTHW)	-	9-Jan-15	7-Jan-16	-	
Action Taken	-	Raised	-	-	
Antenna Height (m)	-	-	-	-	

Frame (ITRF) 2014 to cm precision. Results from PPP are corrected for satellite antenna eccentricity, ocean tidal loading, ionospheric delay, tropospheric delay and antenna phase center variation. ITRF solutions are given in Cartesian Earth-centered Earth-fixed coordinates and are converted to latitude, longitude and height in MATLAB using the World Geodetic System 1984 (WGS84) (Decker). In the next section we will describe the GPS-IR processing from the signal transmission to the final height estimate.

GPS Signal Characteristics

The standard GPS constellation consists of between 24, the minimum for a fully functioning system, to a maximum of 32 satellites or “space vehicles” (SVs) orbiting Earth on six orbital planes. There are currently 31 active SVs in the GPS system. Each SV transmits a unique Gold code, binary sequences designed to correlate poorly with each other and noise, known as a pseudo-random number (PRN) code between 1 and 32. The operational SVs consist of four different generations of satellites, one Block IIA, 11 Block IIR, 7 Block IIR-M, and 12 Block IIF. GPS initially used two L-band frequencies, L1 (1575.42 MHz), and L2 (1227.60 MHz) with a new third frequency, L5 (1176.45 MHz) introduced by Block IIF satellites.

Both carriers, L1 and L2, envelop multiple tracking codes; the two most relevant for GPS-IR being the precision (P) and civilian or coarse acquisition (C or CA) codes, which is only transmitted by L1. The P-code is transmitted on both carriers and encrypted by the W code, which results in the Y code. Civilian receivers cannot decrypt the Y code but by cross-correlating

the L1 and L2 carriers, which both transmit the same Y code, we can determine the relative time difference in the time of flight of the two GPS signals. Cross-correlating L1 and L2, known as semi-codeless tracking, is crucial to GPS operation but comes at the cost of lower SNR L2 phase measurements. To modernize the GPS network, the U.S. Air Force implemented the L2 C code on satellites from Block IIR-M and newer. With the capability to track a code, L2C phase measurement SNR is higher than that of L1 CA code. While higher SNR phase measurements are immensely useful in GPS-IR, they are not reported in the UNAVCO RINEX observation files (the receivers are not programmed to record L2C), so the semi-codeless L2 SNR is used instead.

Multipath signals, reflections from reflectors nearby the antenna, decrease the SNR through interference with the direct signal. To reduce multipath, the Zephyr antenna uses a circular ground plane made of lightweight radar-absorbent material, the same used by Stealth aircraft, in which the electrical resistance of the ground plane increases exponentially with distance from the antenna center causing multipath signals to be resistively dissipated as heat. However, as both the antenna and its multipath mitigating ground plane are not perfect, sufficiently strong multipath signals are recorded to make GPS-IR possible.

GPS-IR

GPS interferometric reflectometry (GPS-IR) is a powerful technique used to determine surface characteristics such as soil moisture content, snow accumulation, and tides in the area around a geodetic GPS station (Bilich et al.; Larson et al.; Nievinski; Shean et al.; Siegfried et al.). GPS-IR began when researchers were studying the signal-to-noise ratio (SNR) data reported by geodetic GPS receivers, shown in Figure 3. They were able to determine that the low elevation periodicity of the SNR is due to the interference between a reflection of the GPS radio signal from the ground surface surrounding the antenna and the direct signal from the GPS satellite. In modeling the periodicity of the SNR, researchers found that the period of the low elevation SNR oscillations is inversely proportional to the height of the antenna relative to the ground surface. Figure 4 shows the model diagram.

The process of GPS-IR starts with incident signals reflected off the ground surface and

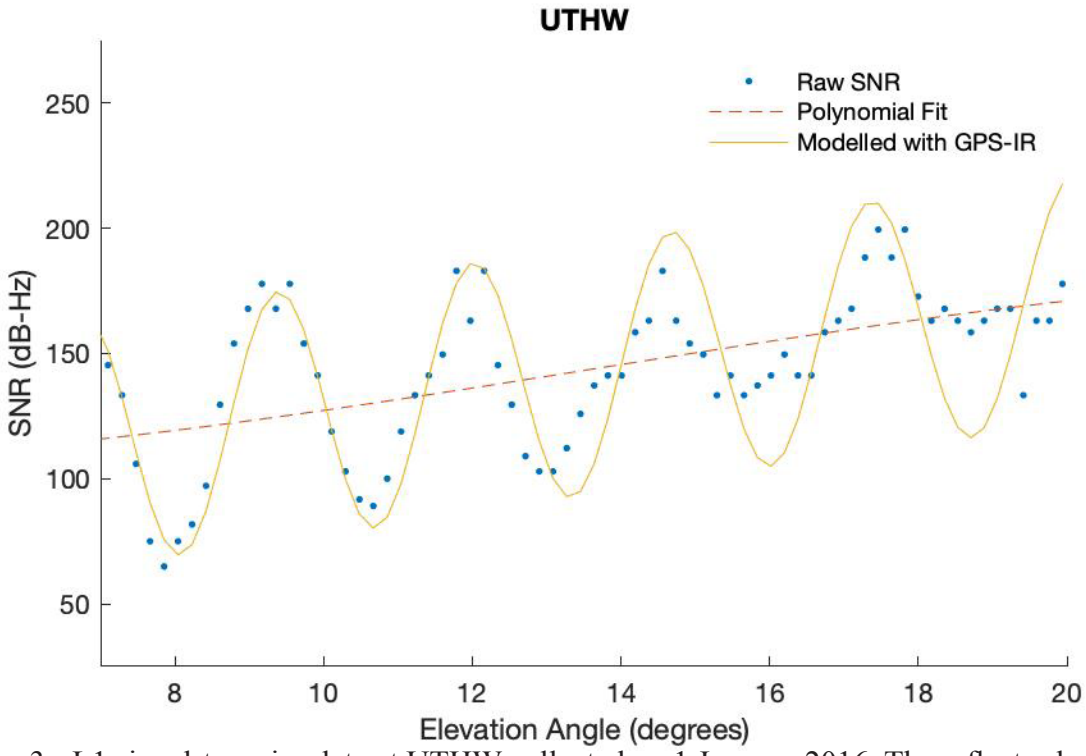

Figure 3 - L1 signal-to-noise data at UTHW collected on 1 January 2016. The reflector height is 2.11 meters.

recorded by the receiver. If the receiver has already locked on to an SV transmitting a PRN code, it will autocorrelate a locally stored version of the PRN code with the one transmitted by the SV. The signal strength is a direct function of the carrier amplitude. Receivers detect multipath that reflects off of surfaces below the antenna ground plane. As an SV passes over the antenna, any multipath from below the antenna will pass in and out of phase with the direct signal creating periodic oscillations in the signal strength, which is then estimated by the receiver and reported in the observation RINEX files. Figure 5 shows the effect of multipath on the SNR of a satellite arc over UTHW; the beginning and end of the time series are where the satellite is at a low elevation angle (below 30 degrees) and multipath is strongest relative to the direct signal. Figure 6 shows the gain pattern for antenna are designed to have maximum gain at zenith and reduced gain at low elevations and below the ground plane. Antenna gain has the most significant effect on the apparent signal strength since the SV transmission power is constant for all azimuths and elevations at the receiver. Unfortunately, there is no standard in reporting signal strength, but both UTHW and LTHW report it in the same way, described in the following paragraph.

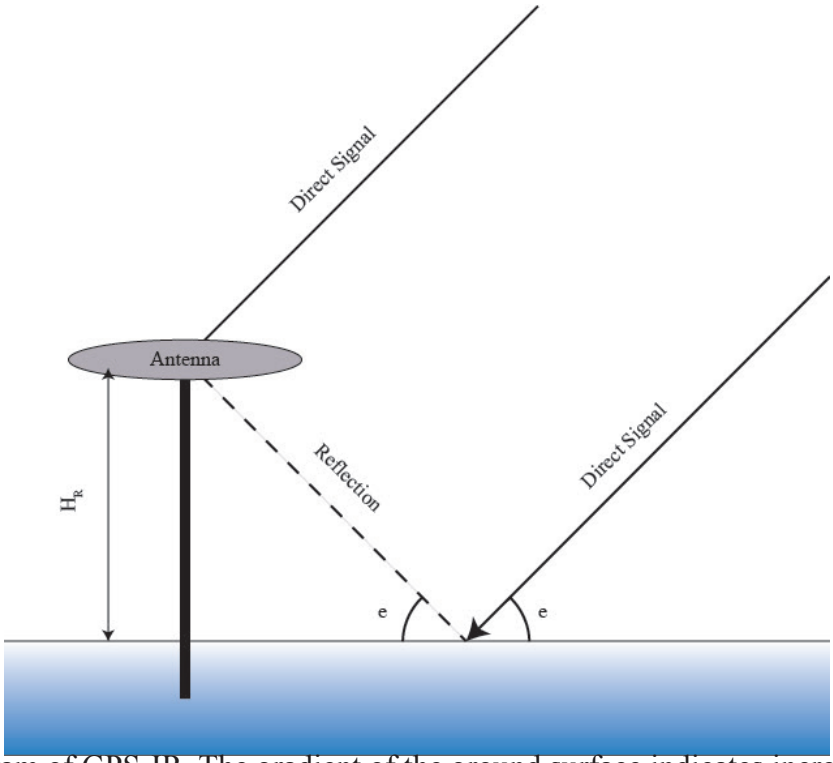

Figure 4 - Diagram of GPS-IR. The gradient of the ground surface indicates increasing density with increasing blueness. Since the distance from the antenna to the satellite is much larger than the length of the reflection, both direct signals are assumed to be parallel. Adapted from Larson et al..

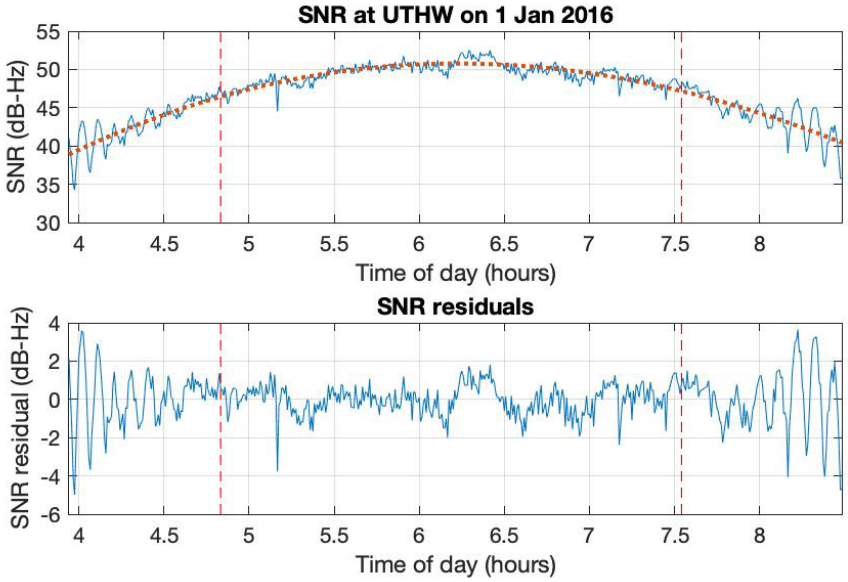

Figure 5 - L1 SNR recorded at UTHW on 1 January 2016 from GPS satellite 23. (top) The modeled direct signal is shown with a dotted line and the SNR is shown in a solid line. Data between the vertical dashed lines is at an elevation angle greater than 30 degrees. (bottom) The modeled direct signal subtracted from the SNR is shown in a solid line. Note the increased magnitude of the SNR residuals at the beginning and end of the time series in addition to their periodic nature.

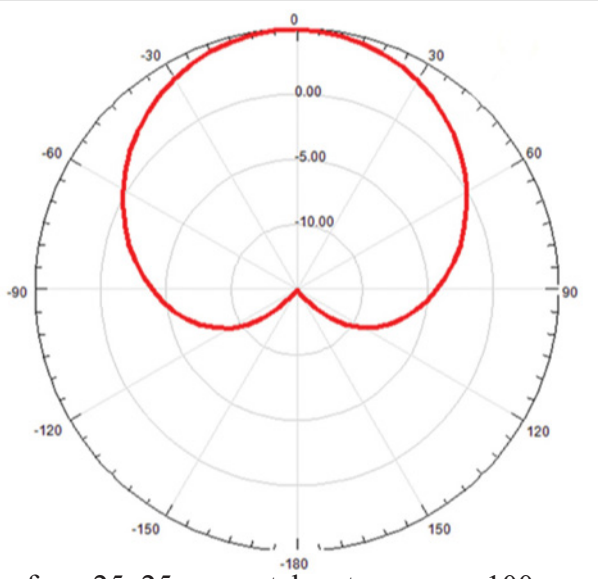

Figure 6 - The gain pattern for a 25x25 mm patch antenna on a 100 mm square ground plane. On the outside of the circle is the elevation relative to the antenna zenith and on the inside of the circle are gain values in dB. Adapted from Panther.

Trimble NetRS receivers report the signal strength as the carrier-to-noise density, also referred to as the SNR. Calculating the true SNR involves finding the power spectral density (PSD) of colored noise and any interference such as jamming (intentional or otherwise). However, to reduce the computational load on the receiver, the effective SNR is determined by using the PSD of thermal noise. The noise, therefore, depends on the temperature within the antenna and receiver, however, the temperature is only measured in the receiver so in reality the noise is estimated using the receiver contribution, ignoring the antenna temperature. The receiver reports the effective SNR in units of decibel-Hertz (dB-Hz) by subtracting the thermal noise power in a 1-Hz bandwidth from the signal power (Kaplan and Hegarty). As both the thermal noise and signal power are reported in logarithmic units (dB), taking the difference between the two values is the ratio.

The signal strength of multipath depends on the reflective properties of the surface. Mirror-like specular reflectors are ideal for GPS-IR as there is minimal power loss in the process of reflecting. A mono-frequency oscillation appears in the SNR when the surface around a GPS antenna is flat, at least semi-mirror-like at L-band frequencies and homogeneous. More research is required to determine the response of snow at L-band frequencies such that we can find the

depth in the snow at which the various GPS signals reflect. Even though we cannot determine the exact depth of the reflection in the snow, we can estimate the area sampled by the reflection using the region around the antenna with the strongest reflection.

Once the receiver records the SNR, any sinusoidal oscillations can be exploited to determine the difference in perpendicular distance from the reflecting surface to the phase center of the antenna. A simple model of the residual SNR (SNR_{res}), after subtracting the direct signal, due to a reflector at height H_R from the antenna is quantified by the following equation (Roesler and Larson):

$$SNR_{res}\left(\sin\left(e\right)\right) = A\left(\sin\left(e\right)\right)\sin\left(\frac{4\pi H_R}{\lambda}\sin\left(e\right) + \phi\right) \quad \text{.....(1)}$$

Where e is the time-dependent elevation of the satellite with respect to the antenna, *A(sin(e))* is the amplitude of the SNR residuals and the two constant variables λ and φ are the carrier wavelength and phase offset of the multipath. The sine of the elevation angle is used as the independent variable in Equation 1. The phase offset is constant during each satellite pass. There are a few implicit assumptions in Equation 1, first and foremost the reflector is assumed to be flat and azimuthally symmetric. Secondly, the amplitude, *A(sin(e))*, cannot be periodic. Equation 1 is valid at UTHW and LTHW as both sites are surrounded by mostly flat, homogeneous snow. The only variations in surface height around the antenna are the frame holding the receiver and wavelike ridges of snow called sastrugi. The sastrugi would introduce noise in the reflector height measurements as the snow surface is not perfectly flat. Averaging the height over all azimuths throughout the day reduces the effect of small scale features found in limited azimuth ranges.

Armed with a description of the GPS network and GPS-IR, we can now delve into the details of preparing and processing SNR data for use with GPS-IR in order to retrieve snow accumulation rates.

Data Processing and Results

Displacement of Thwaites Glacier

Separately from snow accumulation, we fit the station positions in topocentric East, North and up (ENU) using the standard linear trajectory model (SLTM) designed by Bevis and Brown. The SLTM combines three models to fit a GPS time series composed of daily position results: secular trends, instantaneous jumps, and annual. We modeled the secular trends using a quadratic polynomial to capture the acceleration of both stations. Oscillations are fit using a truncated Fourier series solution with annual and semi-annual periods. Finally, a Heaviside function fits the jumps due to raising the antenna (real jumps in antenna position) or changes in the receiver, antenna, or firmware ("processing" jumps). The SLTM models are fit using iteratively re-weighted least squares that down-weights outliers. Figures 7 and 8 show the SLTM results for both UTHW and LTHW respectively. Above each component is the velocity and acceleration at the midpoint of the time series with the annual and semiannual sine and cosine amplitudes and finally the weighted root-mean-square error. In order to better view the oscillations, Figures 9 and 10 show the station positions with the secular terms and jumps removed. Note the inability for the SLTM to completely remove the jumps as it uses the entire dataset in the least-squares calculation so the model has to adjust the jump fits in order to reduce the error in the secular and periodic terms.

Both stations are accelerating North towards the grounding line of Thwaites glacier and traveling East at a fraction of their Northern velocities. UTHW appears to be turning westward as the station weaves through the upper regions of the Thwaites glacier catchment. The stations are descending as they move north towards the grounding line. The WRMS at both sites is surprisingly low when compared to the total distance each station traveled. The maximum error in position at UTHW is 14 centimeters while the station moved by about 1.2 kilometers. At LTHW the maximum error is 1.03 meters over a distance of 2.7 kilometers.

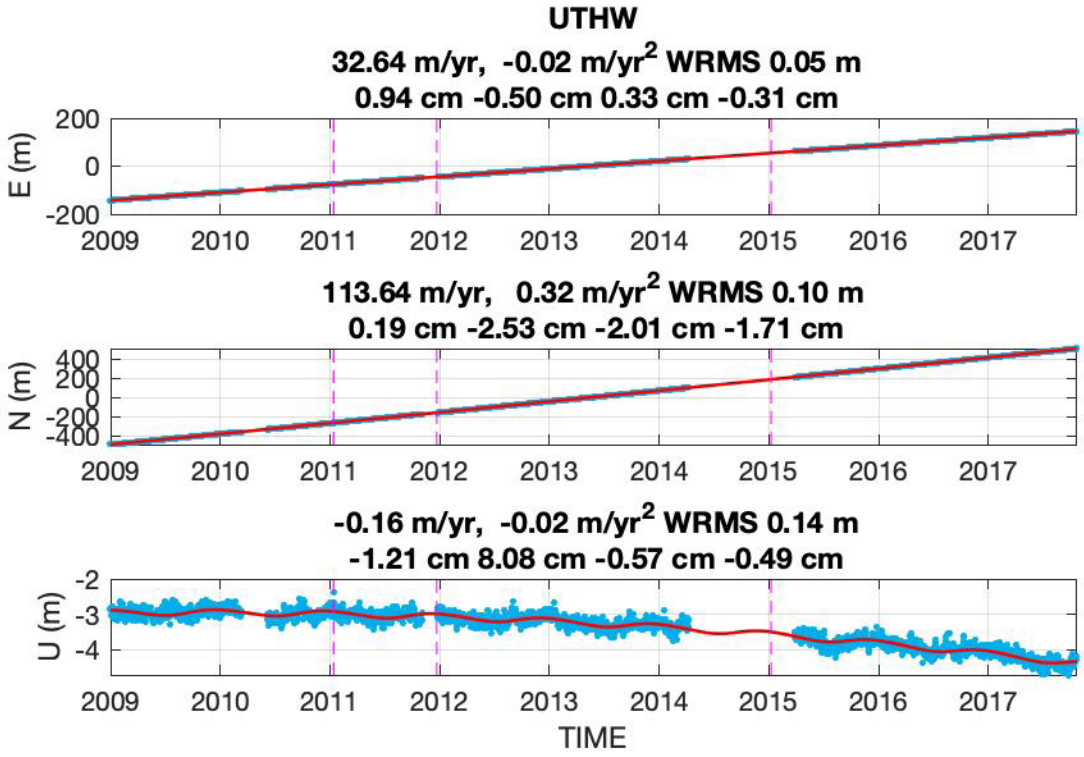

Figure 7 - Position results for UTHW along with the component velocity at the midpoint of the time series and acceleration (top line) with the annual and semiannual sine and cosine amplitudes (bottom line). Also, on the right most of the top line is the weighted root-mean-square error (WRMS) for the component position. The PPP results are in blue while the SLTM is in red.

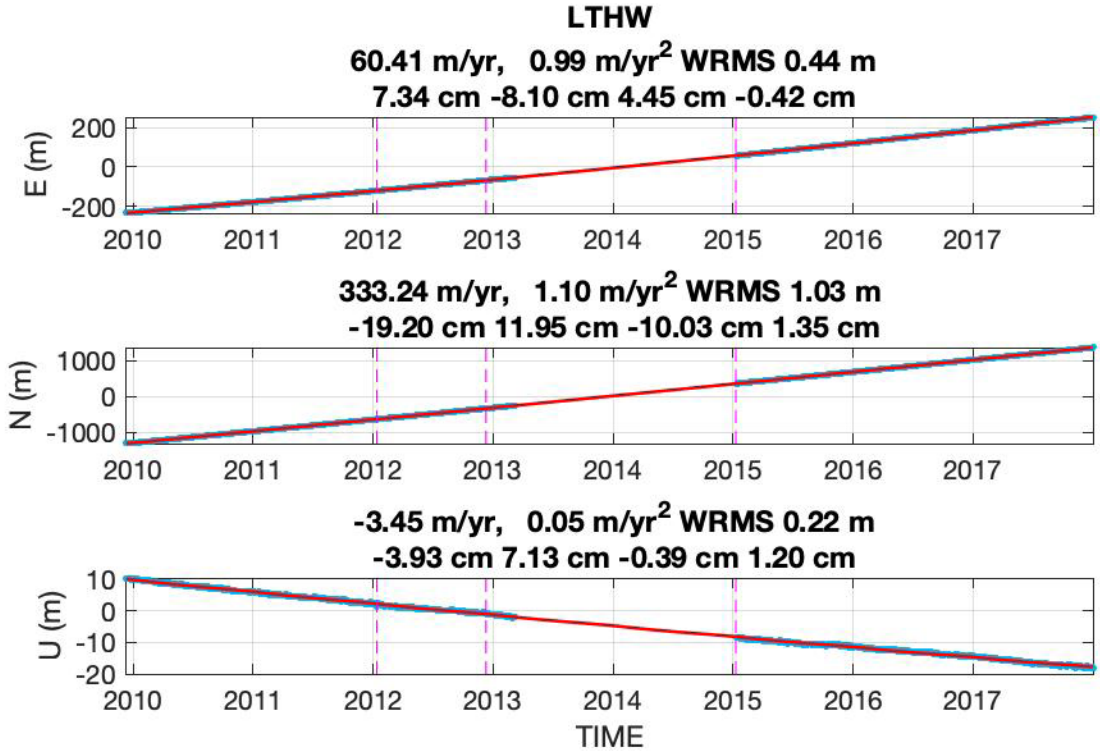

Figure 8 - Position results for LTHW as in Figure 7.

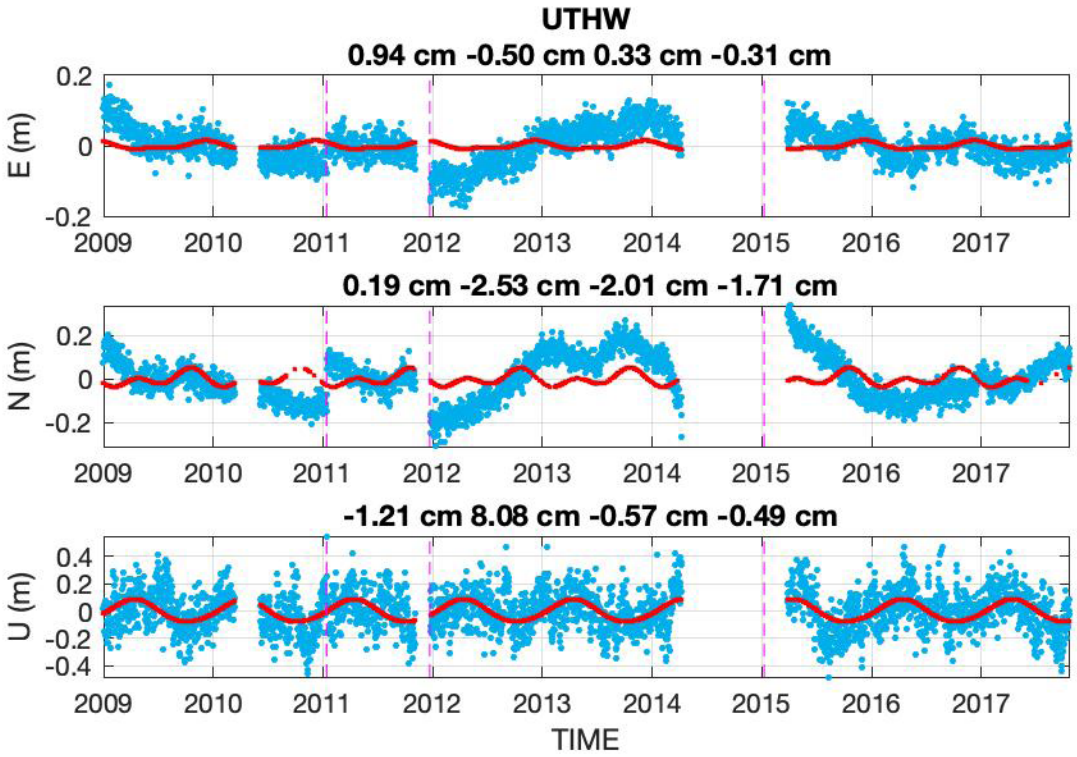

Figure 9 – UTHW displacement with the secular term and jumps removed. Above each plot are the amplitudes for the annual and semi-annual terms.

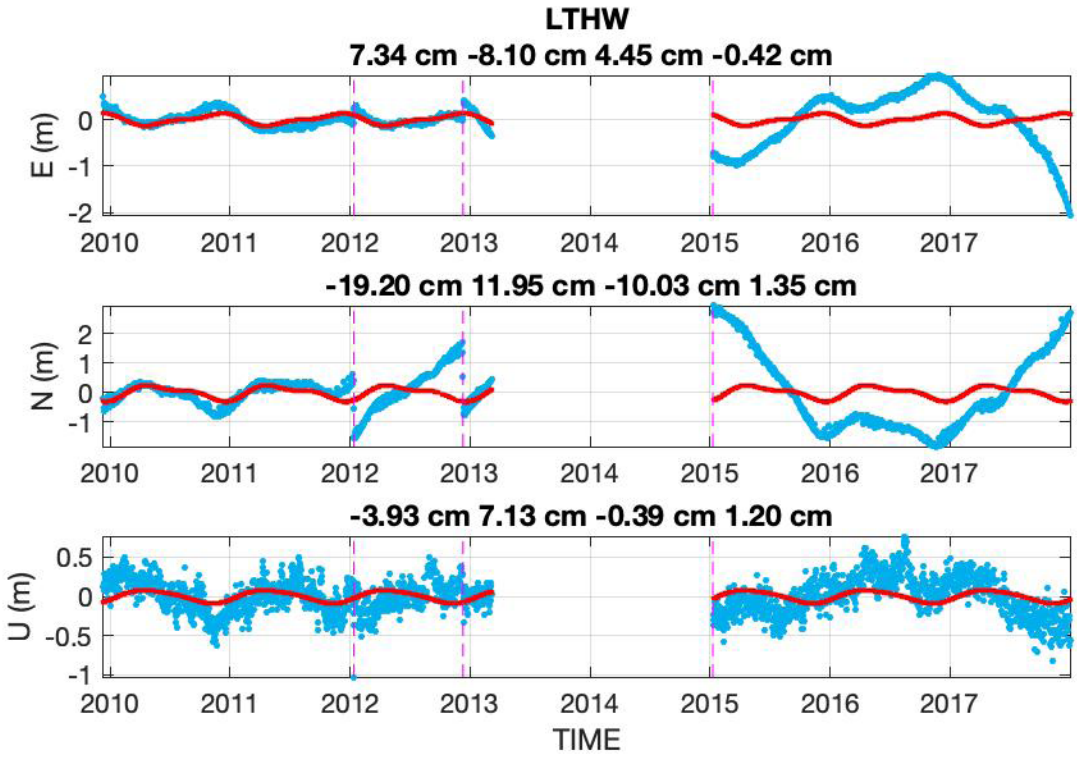

Figure 10 – Periodic terms at LTHW as in Figure 8. At the later half of the East and North components, the secular trend does not fit the data well which makes it difficult to see how well the periodic term fits the data.

Snow Accumulation

Roesler and Larson released a MATLAB toolbox in 2018 which performs the complete GPS-IR processing scheme and is described in this section. First, we selected the SNR data between 5- and 25-degrees elevation and then processed it in empirically determined 45° azimuth bins. Selecting an azimuth bin that is too small will hamper the ability to retrieve a full period of the SNR interference. Likewise, large azimuth bins may contaminate the results by including reflections from areas other than the surface below the antenna in the case of non-uniform ground surfaces. Despite splitting up SV tracks as they cross between bins, we are still able to retrieve a significant number of estimates for H_R. For example, on 1 January 2016, we get 120 estimates for H_R split across azimuth bins. Figure 11 shows the mean H_R estimates for 1 Jan 2016 at LTHW.

The equipment boxes and solar panel frame are located about 5 meters NE of the antenna, where the H_R estimate appears centered on the daily mean indicating that the frame has no significant effect on H_R. It is unclear why there is larger scatter in the estimates in the sector to the NW of the antenna. After limiting the elevation and azimuth, we process the SNR time series for each SV by first finding all the satellite arcs of at least 18-minute-duration (36 samples at 30 second sampling). We approximated the trend in the elevation and azimuth limited SNR by a 3rd order polynomial fit and then subtracted this approximation from the SNR. We then determined the dominant frequency in the elevation windowed SNR data, which corresponds to the reflector height H_R as in Equation 1.

Methods to find the PSD, such as the fast Fourier transform, cannot handle the uneven sampling of the SV arc so we use a method called the Lomb-Scargle Periodogram (LSP) that handles non-uniformly sampled data. Using the LSP is equivalent to using a harmonic least squares fit to the data (Scargle). Two values have to be specified first: the oversampling (OFAC) and high frequency (HIFAC) factors. The OFAC sets the frequency resolution and the HIFAC serves as the Nyquist frequency in the LSP. In GPS-IR the OFAC is based on the desired precision of H_R that is set to 6 centimeters based on results from Siegfried et al. where they found that the error between true H_R as measured in situ and GPS-IR H_R have a standard deviation of

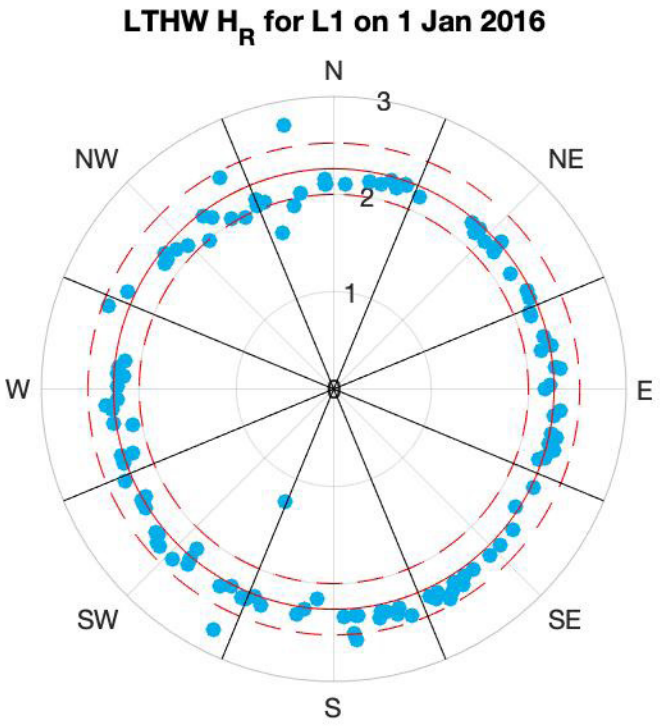

Figure 11 - H_R values (blue) from LTHW on 1 January 2016 sorted by azimuth bin (black). The radius represents reflector height values with a radius of zero corresponding to a height of zero. The H_R values are placed at their mean azimuth. The daily mean is shown as a solid red line with two standard deviations in dashed red.

about 6 centimeters. The high-frequency factor determines the maximum frequency in the LSP, and in GPS-IR this corresponds to the maximum height that can be estimated from the input data. In this study the maximum height is arbitrarily set to 5 meters. We then find the peak power from the suite of LSP results. In order to decrease the variability in H_R, a noise floor is determined based on the average power of the LSP during a single SV arc. Values of H_R from a single SV arc are only considered if the peak power is at least two times the noise floor. If the peak power meets these conditions, the value of H_R is accepted and all accepted values of H_R for the day are averaged. The uncertainty in the estimation of the daily H_R is determined by finding the standard deviation. Figure 12 shows the suite of results from the LSP from a single day of data at LTHW in addition to a histogram of the results. It appears that the distribution is Gaussian.

To estimate the snow accumulation rate we first set a 0 datum using the mean height for the first 30 days of data using the following equation from Siegfried et al.:

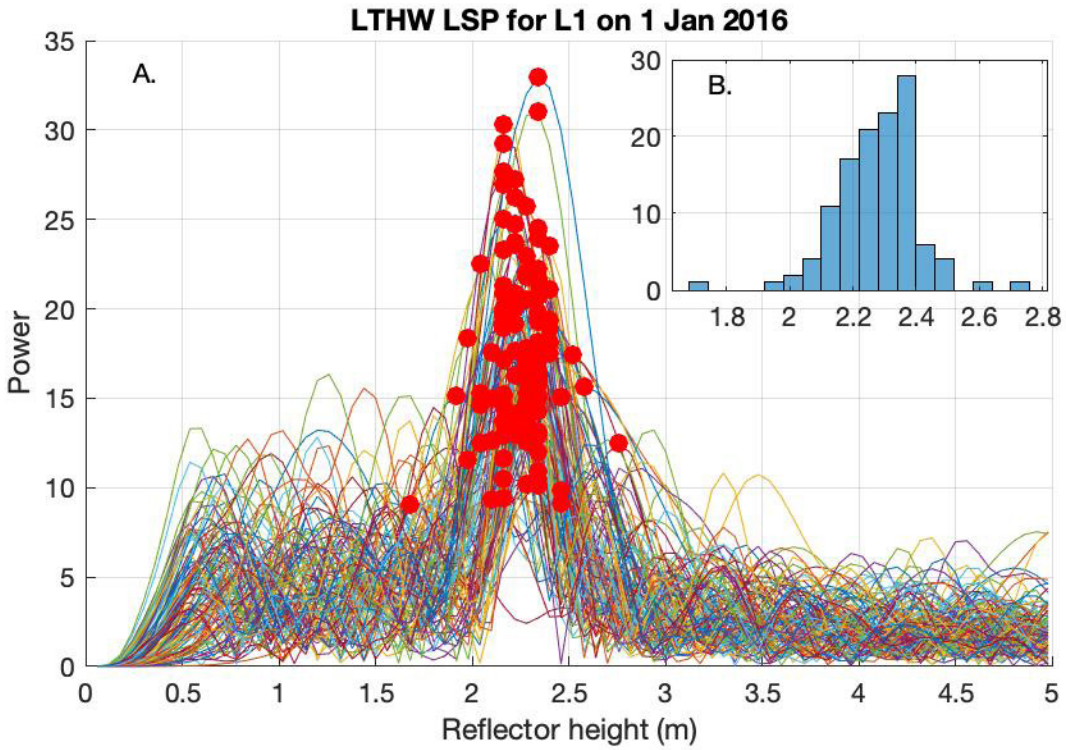

Figure 12 – A. L1 Lomb-Scargle periodogram of SNR for each satellite arc from 5 to 25 degrees elevation for LTHW on 1 Jan 2016. The markers indicate a valid result for the reflector height which are then averaged for to return the day's reflector height. B. histogram of reflector height with bins spaced at 6 centimeters.

$$\Delta H_S(t_n) = -H_R(t_n) + \sum_{m=1}^{30} H_R(t_m) \quad \text{.....(2)}$$

It is important to note a few assumptions made in using $\Delta H_S(t_n)$ for snow accumulation rates. First, the firn compaction between the base of the antenna and the surface must be less than the resolution of $\Delta H_S(t_n)$. While firn compresses the fastest at shallow depths, it still only compresses at millimeters per year. An estimate of the firn compaction rate is determined to be about 1.5 mm/yr using 24 average accumulation rates from Medley et al. and the firn model by Helsen et al. that is calibrated for Western Antarctica. We also do not account for sublimation or ablation. Snow accumulation results are shown in Figure 13 for both L1 and L2 along with the ERA5 dataset described in the following section after converting to m.w.e. per year by multiplying daily accumulation by the appropriate ratio of surface density to water. Here we used

approximate surface densities from Grima et al. for UTHW (450 kg/m3) and LTHW (500 kg/m3). The velocity in the secular component of SLTM is used in determining snow accumulation rates. While the SLTM was not originally designed for use in snow accumulation studies, we are able to put to use each component in order to achieve accurate rates. Table 2 shows our snow accumulation rate estimates.

Snow Accumulation Models

Three independent sources of data are used to compare GPS-IR results for snow accumulation on Thwaites glacier, airborne radar data combined with ice cores, a global forecast reanalysis and results presented at the 2016 AGU Fall meeting (Hersbach and Dee; Medley et al.; Rodriguez-Morales et al.; Shean et al.). The combination of airborne radar data and ice core analysis was performed using two Center for Remote Sensing of Ice Sheets (CReSIS) Twin Otter mounted radars and ten ice cores extracted from different areas of Thwaites and Pine Island glaciers in a study by Medley et al.. The stratigraphy of the ice cores was then correlated with an age scale using isotope analysis. Horizons in the ice cores were mapped across Thwaites glacier by analyzing the reflections of the CReSIS radar. Once the firn horizons were mapped, both the depth below the surface and ages were used to determine the amount of accumulation. Results represent a 24-year average accumulation rate for the Thwaites glacier gridded to 3x3 km cells. Despite the relatively high resolution of the grid compared to other accumulation models, it is smoothed using a 9x9 cell mean filter in order to reduce the high-frequency interpolation artifacts. The European Centre for Medium-Range Weather Forecasts (ECMWF) is a multinational organization that develops forecast models for use across the globe. Every few years the ECMWF combines their forecast models with observational data in the form of reanalysis products. ECMWF Reanalysis 5 (ERA5) began development in January of 2016 in order to create a comprehensive global dataset on 330 different atmospheric parameters. The observational data consists of results from 55 different satellites and 15 different types of in-situ measurements. The global horizontal resolution is 31 km, and the atmospheric pressure levels are divided up into 137 levels between surface pressure to 0.01 hPa. Data on snow accumulation is

Table 2 - Snow accumulation values for L1, L2, ERA5, Medley et al. and Shean et al.. All values for snow accumulation are in m.w.e per year.

Station	L1	L2	ERA5	Medley et. al. 2014	Shean et. al. 2016
UTHW (m/yr)	0.44 ± 0.03	0.47 ± 0.04	0.44 ± 0.02	0.48 ± 0.02	0.48 ± 0.14
LTHW (m/yr)	0.56 ± 0.06	0.59 ± 0.06	0.58 ± 0.04	0.54 ± 0.03	0.49 ± 0.14

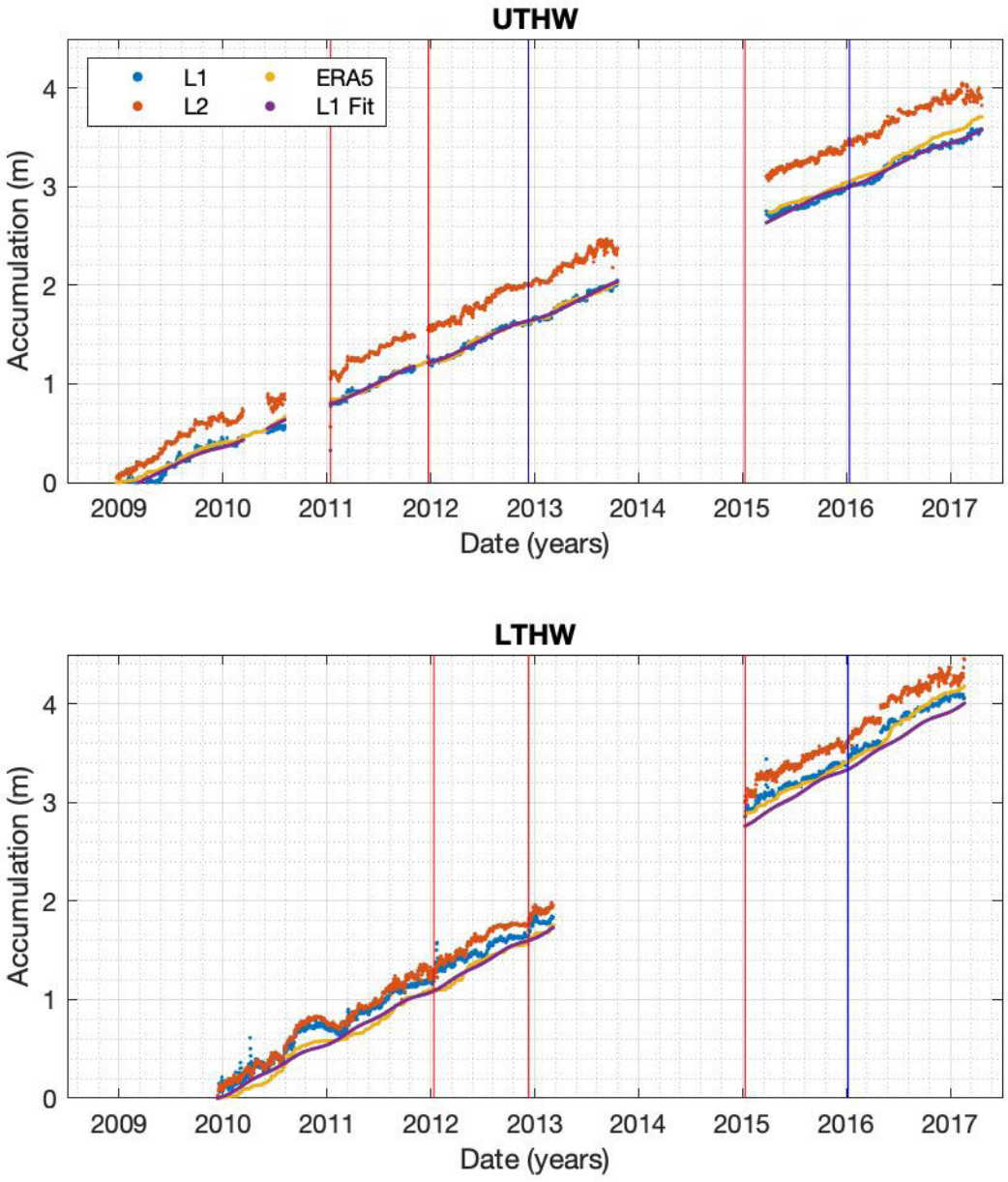

Figure 13 – Snow accumulation results for UTHW and LTHW along with the ERA5 model. The accumulation is measured in meters water equivalent using the density from Grima et al.. Vertical lines represent site visits as shown in Table 1. The L1 fit is not drawn when there is no corresponding data.

available from 1979 until the present in hourly format (Hersbach and Dee). Operational snow-depth analysis has been conducted at the ECMWF since 1987 using a successive correction method and compared to the MODIS snow cover radar (Drusch et al.). Snowfall data collected for the research presented here was retrieved hourly in (m.w.e). The hourly data was then integrated over the same time periods reported by GPS-IR results for both sites. The rate was determined similarly to how our GPS-IR results were found, using the SLTM.

Accumulation rates were also derived by Shean et al. when studying the surface mass balance of Pine Island Glacier (PIG). The results were presented at the 2016 AGU meeting but were not included in the paper published in 2017. No errors were presented, so errors were approximated from the 2017 paper which used similar techniques to derive snow accumulation.

Discussion

Many phenomena can cause a glacier to change velocity such as ice calving, change in the basal melt, and active sub-glacial lakes. Some recent velocity changes at the surface of Thwaites glacier have been explained as the result of sub-glacial lakes actively filling and draining over a period of years (Smith et al.). As the lakes filled with water, the basal stress of the glacier is reduced allowing the glacier to flow more freely and thus increasing its velocity. When a sub-glacial lake drains the basal stress increases, which in turn slows down the glacier. Evidence of filling and draining can be seen in the residuals of the horizontal components at LTHW and to a lesser extent UTHW (Hoffman et al.). By using a quadratic in the secular component of the SLTM, we can test for deviations from constant acceleration in the SLTM residuals. It appears that the quadratic fit cannot model the data after 2015; in fact, LTHW seems to be traveling North faster than the SLTM model as if the glacier suddenly sped up. The glacier speeding up around LTHW is consistent with the theory that the nearby sub-glacial lake THW_{124} is now filling, after its drainage during 2013 (Smith et al.). Unfortunately, we cannot determine whether LTHW slowed down during the 2013 drainage event indicating the relationship between the displacement of LTHW and the sub-glacial lake THW_{124}. If the large position residuals were due to another phenomenon, such as calving of the ice shelf, then similar signals would

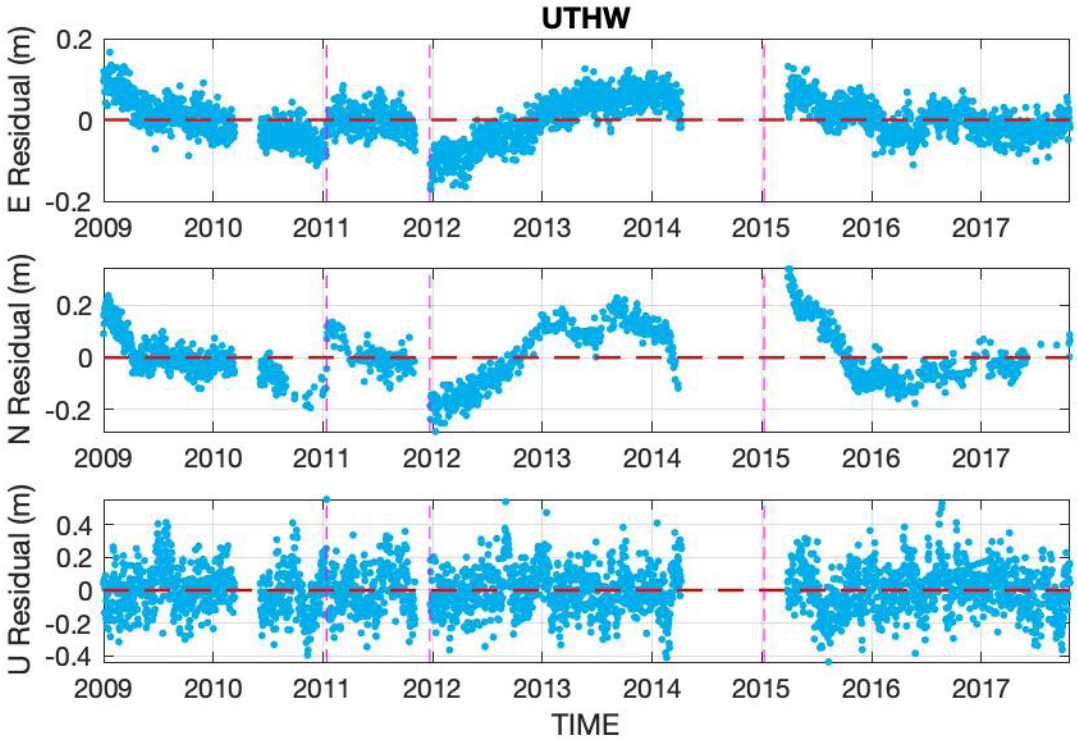

Figure 14 – SLTM position residuals at UTHW.

presumably be seen at both UTHW and LTHW. Without similar position residuals, localized events seem to be the best explanation for the deviations for the SLTM fit. Figures 14 and 15 show the SLTM residuals at both stations.

If we were to apply the same logic to UTHW, that the drainage or filling of a sub-glacial lake causes large SLTM residuals, then it would seem that there may be a nearby lake that had filled slightly after 2015. The North component of UTHW experienced a minor increase in acceleration after 2015; however, the station then recovers and closely mirrors the SLTM after 2016. The remainder of this section focuses on the GPS-IR results.

L1 and L2 return different snow heights indicating different penetration depths. L2 also returns higher accumulation rate compared to L1. Regarding the increased accumulation, L2 could be reflecting off an interface within the firn that is deeper than the one sampled by L1, which is supported by a mean increase in snow height of 4.7 centimeters. The more concerning contrast between L1 and L2 is the discrepancy in the rate of snow accumulation. The discrepancy indicates that the surface which L2 reflects off of is rising faster than the L1 reflector by 4.4

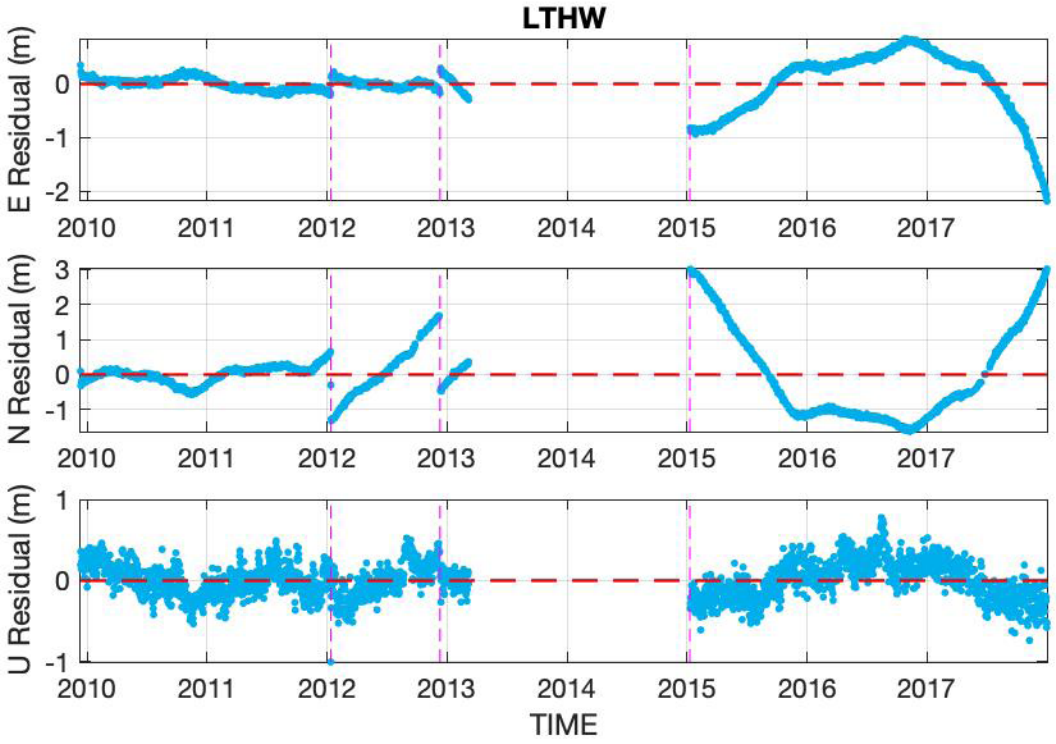

Figure 15 - SLTM position residuals at LTHW. The magnitudes of the component residuals are much greater than at UTHW. LTHW appears to have a greater North acceleration after 2015 while the up component does not deviate very much from the SLTM model.

and 3.6 centimeters per year at UTHW and LTHW respectively. The rate increase is counter-intuitive when taken into consideration with the accumulation bias towards L2, if L2 is sampling deeper in the firn than L1, then L1 should also be influenced by the rate increase seen by L2. The remaining discussion focuses on the results from L1 due to the inconsistencies in the L2 results.

Figure 16 shows the snow accumulation SLTM residuals with zoomed in figures during intervals when data was recorded at both UTHW and LTHW. Accumulation residuals from both stations approximately track each other with infrequent variations, usually with LTHW deviating from the mean at a higher value than UTHW. The significant deviations at LTHW sometimes make their way to UTHW and when they do it is usually delayed by a few days and at a reduced magnitude. The delay may be due to storms making their way from LTHW to UTHW, a distance of 129.4 kilometers.

While occasionally offset from the model, L1 almost precisely matches the ERA5 snowfall rates at both sites. The offset is not constant through time which is to be expected since

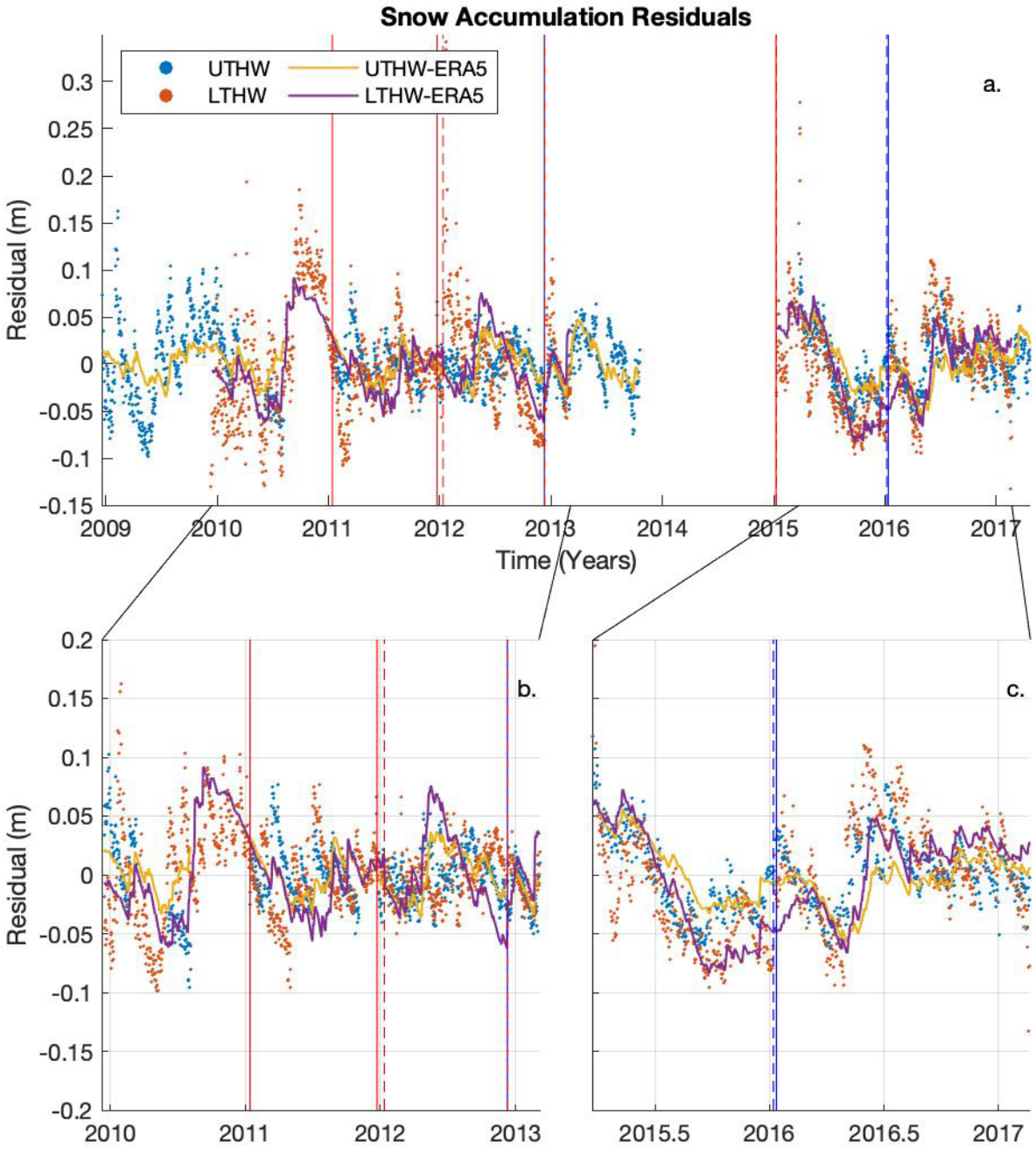

Figure 16 - L1 snow accumulation residuals at both UTHW and LTHW. a. shows the entire dataset for both stations; b. and c. show the time series where data were recorded simultaneously at both sites. ERA5 accumulation residuals for both stations are also plotted in each figure. The vertical lines correspond to the site visits as shown in the previous figures with the LTHW visits in dashed lines and UTHW in solid lines.

the ERA5 dataset is over a grid with 31-kilometer spacing so L1 GPS-IR results will detect small-scale variations in snow accumulation. ERA5 consistently estimates lower accumulation rates, by an average of 2.5 and 4.1 centimeters respectively, at UTHW and LTHW. Perhaps with the increased interest in snow accumulation retrieval via GPS-IR, results from UTHW and LTHW can be incorporated into the next reanalysis product.

Comparing L1 accumulation rates to those found by Medley et al. shows that accumulation at UTHW has decreased by 3.7 centimeters per year while simultaneously increasing at LTHW by 4.5 centimeters per year. Accumulation rates found in the similar GPS-IR study match both the results found here and other models for UTHW, however, the results from their study for LTHW differ from the others. The primary reason for this discrepancy could be due to how antenna changes were dealt with in their study but, without further information, we cannot be sure of the exact reason.

LTHW has the highest snow accumulation SLTM residual during the latter half of 2010. It appears that there was an approximately 40-centimeter increase in snowfall which was subsequently ablated throughout 2011. Wind velocity, as recorded by the MET pack located on the receiver frame, indicates an average speed of 8.1 meters per second during 2010, half a meter per second greater than the 7-year average of 7.6 meters per second and .8 meters per second greater than the following years average. The rapid accumulation in 2010 may not have been able to harden through isothermal sintering quickly enough to remain in place leading to higher than usual ablation in 2011.

UTHW has a much lower average wind velocity of 6.3 meters per second over its 8-year history. Variability in the wind velocity is low, similar to the snow accumulation. UTHW experiences less storm activity than LTHW, a fact supported by both decreased accumulation rates and wind velocities.

Conclusions

The SLTM was used to determine the direction and velocity of both stations. In coming years, both UTHW and LTHW will be valuable stations in monitoring the horizontal velocity

and snow accumulation on Thwaites glacier. By examining the SLTM residuals, it is apparent that LTHW is experiencing local accelerations due to the apparent filling and draining of a nearby sub-glacial lake THW_{124}. Both stations were used to determine 8- and 7-year average snow accumulation rates using GPS-IR on L1 and L2. Results from L2 are inconsistent with L1 indicating that L2 is not a viable source for GPS-IR processing. However, L1 rates accurately track model estimates from ERA5 and vary only slightly from the 24-year average found by Medley et al. . Increased accumulation rates at LTHW and decreased rates at UTHW suggest a shift in snow accumulation distribution on Thwaites glacier from inland towards the ASE. Variations from the mean accumulation rate at both sites can be correlated with wind velocity records from in situ MET pack data to help identify ablation events. Modernization of the GPS constellation by the U.S. Air Force will improve GPS-IR capabilities by adding more tracking codes on both L1 and L2 in addition to another carrier L5, making GPS-IR an essential technique to follow in the coming years.

Data Sources

Observational, navigation and meteorological GPS data was retrieved from the UNAVCO facility through the Geodetic Data Services program. www.unavco.org. Antarctica-POLENET GPS Network - UTHW-Up Thwaites Glacier P.S. DOI: https://doi.org/10.7283/T50P0XBC. Antarctica-POLENET GPS Network - LTHW-Lower Thwaites Glacier P.S. DOI: https://doi.org/10.7283/T5NK3C7D. ECMWF ERA5 single level data from 2000 to the present was accessed using the Climate Data Store. cds.climate.copernicus.eu DOI: https://doi.org/10.5065/D6X34W69

References

Barletta, Valentina R et al. "Observed Rapid Bedrock Uplift in Amundsen Sea Embayment Promotes Ice-Sheet Stability." Science, vol. 360, no. 6395, 2018, pp. 1335-1339.

Bevis, Michael and Abel Brown. "Trajectory Models and Reference Frames for Crustal Motion Geodesy." Journal of Geodesy, vol. 88, no. 3, 2014, pp. 283-311, doi:10.1007/s00190-013-0685-5.

Bilich, Andria et al. "Scientific Utility of the Signal-to-Noise Ratio (SNR) Reported by Geodetic GPS Receivers." Proc. ION GNSS, Conference Presentation.

Decker, B LOUIS. "World Geodetic System 1984." Defense Mapping Agency Aerospace Center St Louis Afs Mo, 1986.

Dow, C. F. et al. "Dynamics of Active Subglacial Lakes in Recovery Ice Stream." Journal of Geophysical Research: Earth Surface, vol. 123, no. 4, 2018, pp. 837-850, doi:10.1002/2017jf004409.

Drusch, Matthias et al. "ECMWF's Global Snow Analysis: Assessment and Revision Based on Satellite Observations." Journal of Applied Meteorology, vol. 43, no. 9, 2004, pp. 1282-1294.

Greene, Chad A et al. "Antarctic Mapping Tools for Matlab." Computers & Geosciences, vol. 104, 2017, pp. 151-157.

Grima, Cyril et al. "Surface Slope Control on Firn Density at Thwaites Glacier, West Antarctica: Results from Airborne Radar Sounding." Geophysical Research Letters, vol. 41, no. 19, 2014, pp. 6787-6794, doi:10.1002/2014gl061635.

Gurtner, Werner and Lou Estey. "Rinex-the Receiver Independent Exchange Format-Version 3.00." Astronomical Institute, University of Bern and UNAVCO, Boulder, Colorado., 2007.

Helsen, Michiel M et al. "Elevation Changes in Antarctica Mainly Determined by Accumulation Variability." Science, vol. 320, no. 5883, 2008, pp. 1626-1629.

Hersbach, H and D Dee. "Era5 Reanalysis Is in Production." ECMWF newsletter, vol. 147, no. 7, 2016.

Hoffman, Andrew O. et al. "Interannual to Subdaily Fluctuations in Thwaites Glacier Speed Associated with Ocean Forcing and Calving." AGU Fall Meeting Abstracts, Conference Presentation.

Kaplan, Elliott and Christopher Hegarty. Understanding Gps: Principles and Applications. Artech house, 2005.

Larson, Kristine M. et al. "Constraints on Snow Accumulation and Firn Density in Greenland

Using GPS Receivers." Journal of Glaciology, vol. 61, no. 225, 2017, pp. 101-114, doi:10.3189/2015JoG14J130.

Medley, B. et al. "Constraining the Recent Mass Balance of Pine Island and Thwaites Glaciers, West Antarctica, with Airborne Observations of Snow Accumulation." The Cryosphere, vol. 8, no. 4, 2014, pp. 1375-1392, doi:10.5194/tc-8-1375-2014.

Nievinski, Felipe Geremia. "Forward and Inverse Modeling of Gps Multipath for Snow Monitoring." 2013.

Panther, Gyles. "Patch Antennas for the New GNSS." GPS World, 2012.

Rignot, Eric et al. "Recent Antarctic Ice Mass Loss from Radar Interferometry and Regional Climate Modelling." Nature Geoscience, vol. 1, no. 2, 2008, p. 106.

Rodriguez-Morales, Fernando et al. "Advanced Multifrequency Radar Instrumentation for Polar Research." IEEE Transactions on Geoscience and Remote Sensing, vol. 52, no. 5, 2014, pp. 2824-2842.

Roesler, Carolyn and Kristine M Larson. "Software Tools for Gnss Interferometric Reflectometry (GNSS-IR)." GPS Solutions, vol. 22, no. 3, 2018, p. 80.

Scambos, T. A. et al. "How Much, How Fast?: A Science Review and Outlook for Research on the Instability of Antarctica's Thwaites Glacier in the 21st Century." Global and Planetary Change, vol. 153, 2017, pp. 16-34, doi:10.1016/j.gloplacha.2017.04.008.

Scargle, Jeffrey D. "Studies in Astronomical Time Series Analysis. II-Statistical Aspects of Spectral Analysis of Unevenly Spaced Data." The Astrophysical Journal, vol. 263, 1982, pp. 835-853.

Shean, David E. et al. "In-Situ Gps Records of Surface Mass Balance, Firn Compaction Rates, and Ice-Shelf Basal Melt Rates for Pine Island Glacier, Antarctica." AGU Fall Meeting Abstracts, 12 December 2016, Moscone Center, San Francisco, CA, Conference Presentation.

Shean, David E. et al. "GPS-Derived Estimates of Surface Mass Balance and Ocean-Induced Basal Melt for Pine Island Glacier Ice Shelf, Antarctica." The Cryosphere, vol. 11, no. 6, 2017, pp. 2655-2674, doi:10.5194/tc-11-2655-2017.

Siegfried, M. R. et al. "Snow Accumulation Variability on a West Antarctic Ice Stream Observed with Gps Reflectometry, 2007-2017." Geophysical Research Letters, vol. 44, no. 15, 2017, pp. 7808-7816, doi:10.1002/2017gl074039.

Smith, Benjamin E. et al. "Connected Subglacial Lake Drainage beneath Thwaites Glacier, West Antarctica." The Cryosphere Discussions, 2016, pp. 1-19, doi:10.5194/tc-2016-180.

Wright, Andrew and Martin Siegert. "A Fourth Inventory of Antarctic Subglacial Lakes."

Antarctic Science, vol. 24, no. 06, 2012, pp. 659-664, doi:10.1017/s095410201200048x.

Zwally, H Jay et al. “Antarctic and Greenland Drainage Systems.” GSFC Cryospheric Sciences Laboratory, 2012.